Dynamical Density Functional Study of Acetylene to Vinylidene Isomerization in $(Cp)(CO)_2Mn(HC{\equiv}CH)$

Filippo De Angelis and Antonio Sgamellotti*

Istituto di Scienze e Tecnologie Molecolari (ISTM-CNR) c/o Dipartimento di Chimica, Università di Perugia, I-06123 Perugia, Italy

Nazzareno Re

Facoltà di Farmacia, Università G. D'Annunzio, I-66100 Chieti, Italy

Received October 31, 2001

The acetylene to vinylidene isomerization in $(Cp)(CO)_2Mn(HC{\equiv}CH)$ has been investigated by both static and dynamic density functional calculations. The potential energy surface for the conversion of coordinated acetylene to vinylidene has been analyzed by a gradient-corrected DFT approach. The η^1-vinylidene complex has been found 9.0 kcal mol^{-1} more stable than the acetylene complex and is the thermodynamically most stable species of this reaction system. An unprecedented η^2-vinylidene species has been characterized and found 38.4 kcal mol^{-1} higher than the corresponding η^1-isomer. The direct 1,2 hydrogen shift, proceeding via an agostic intermediate, is the energetically most favorable path, with a free energy barrier of 27.3 kcal mol^{-1}. The higher barrier computed for the oxidative addition leading to the corresponding alkynylhydrido complex (35.0 kcal mol^{-1}) rules out the intermediacy of such a species in the investigated process. Dynamics simulations have also been performed on the $(Cp)(CO)_2Mn(HC{\equiv}CH)$ complex in order to study the detailed features of the possible acetylene to vinylidene conversion pathways and show that the isomerization effectively takes place through a direct 1,2 hydrogen shift from the agostic intermediate.

1. Introduction

The reactivity of unsatured hydrocarbons on transition metals centers is currently a topic of great interest in both homogeneous and heterogeneous catalysis.[1]

In particular, the acetylene−vinylidene rearrangement in the coordination sphere of a transition metal has attracted much interest from both an experimental[2] and theoretical point of view.[3] While the formation of vinylidene from free acetylene is a strongly endothermic (44−47 kcal mol^{-1}) process,[2] the relative energies of the two isomers change dramatically in the coordination sphere of several transition metals. Metal vinylidenes are stable complexes and may be more stable than the corresponding acetylene isomers.[4]

Two different mechanism have been proposed for the metal-assisted isomerization of 1-alkyne to vinylidene (see Scheme 1). One is essentially the same mechanism occurring in the free acetylene−vinylidene tautomerization, with an approach of the metal to C_α and a concomitant 1,2 hydrogen shift from C_α to C_β (path 1A in Scheme 1). On the basis of photochemical studies on manganese and rhenium vinylidene complexes,[5] Antonova et al. proposed an alternative mechanism in which an oxidative addition of the 1-alkyne to the metal center gives an alkynylhydrido complex, which then isomerizes by a 1,3 hydrogen shift from the metal to C_β (path 2 in Scheme 1). The first theoretical investigation to this discussion was the work by Silvestre and Hoffmann at the extended Hückel level on the acetylene to vinylidene isomerization in the $(Cp)(CO)_2Mn(HC{\equiv}CH)$ complex.[6] Their calculations showed that the 1,3 hydrogen shift in path 2 has a high activation barrier and suggested that the rearrangement proceeds through path 1A with a direct 1,2 hydrogen shift. More accurate information on the mechanism of this rearrangement came from the theoretical work of Wakatsuki et al. on the $[Cl_2Ru(PH_3)_2(HC{\equiv}CH)]^+$ complex.[7] Their calculations showed that for the acetylene−vinylidene rearrangement in this ruthenium(II) d^6 complex the 1,2-hydrogen shift is kinetically favored and indicated that the metal acetylene complex rearranges in a slippage

(1) Cotton, F. A.; Wilkinson, G. *Advanced Inorganic Chemistry*, 5th ed.; Wiley-Interscience: New York, 1988. Bruce, M. I. *Chem. Rev.* **1998**, *98*, 2797. Zaera, F. *Chem. Rev.* **1995**, *95*, 2651.

(2) Chen, Y.; Jonas, D. M.; Hamilton, C. E.; Green, P. G.; Kinsey, J. L.; Field, R. W. *Ber. Bunsen-Ges. Phys. Chem.* **1988**, *92*, 329. Chen, Y.; Jonas, D. M.; Kinsey, J. L.; Field, R. W. *J. Chem. Phys.* **1989**, *91*, 3976. Erwin, K. M.; Ho, J.; Lineberger, W. C. *J. Chem. Phys.* **1989**, *91*, 5974. Erwin, K. M.; Gronert, S.; Barlow, S. E.; Gilles, M. K.; Harrison, A. G.; Bierbaum, V. M.; DePuy, C. H.; Lineberger, W. C.; Ellison, G. B. *J. Am. Chem. Soc.* **1990**, *112*, 5750.

(3) Carrington, T.; Hubbard, L. M.; Schaefer, H. F.; Miller, W. H. *J. Chem. Phys.* **1984**, *80*, 4347. Gallo, M. M.; Hamilton, T. P.; Schaefer, H. F. *J. Am. Chem. Soc.* **1990**, *112*, 8714. Peterson, G. A.; Tensfeldt, T. G.; Montgomery, J. A., Jr. *J. Am. Chem. Soc.* **1992**, *114*, 6133. Jensen, J. H.; Morokuma, K.; Gordon, M. S. *J. Chem. Phys.* **1994**, *110*, 1981.

(4) Werner, H. *Angew. Chem, Int. Ed. Engl.* **1990**, *29*, 1077. Bruce, M. I. *Chem. Rev.* **1991**, *91*, 197.

(5) Nesmeyanov, A. N.; Alexandrov, G. G.; Antonova, A. B.; Anisimov, K. N.; Kolobova, N. E.; Struchkov, Yu. T. *J. Organomet. Chem.* **1976**, *110*, C36. Antonova, A. B.; Kolobova, N. E.; Petrovsky, P. V.; Lokshin, B. V.; Obezyuk, N. S. *J. Organomet. Chem.* **1977**, *137*, 55.

(6) Silvestre, J.; Hoffmann, R. *Helv. Chim. Acta* **1985**, *68*, 1461.

(7) Wakatsuki, Y.; Koga, N.; Yamazaki, H.; Morokuma, K. *J. Am. Chem. Soc.* **1994**, *116*, 8105.

10.1021/om010943k CCC: $22.00
Publication on Web 05/18/2002

Scheme 1

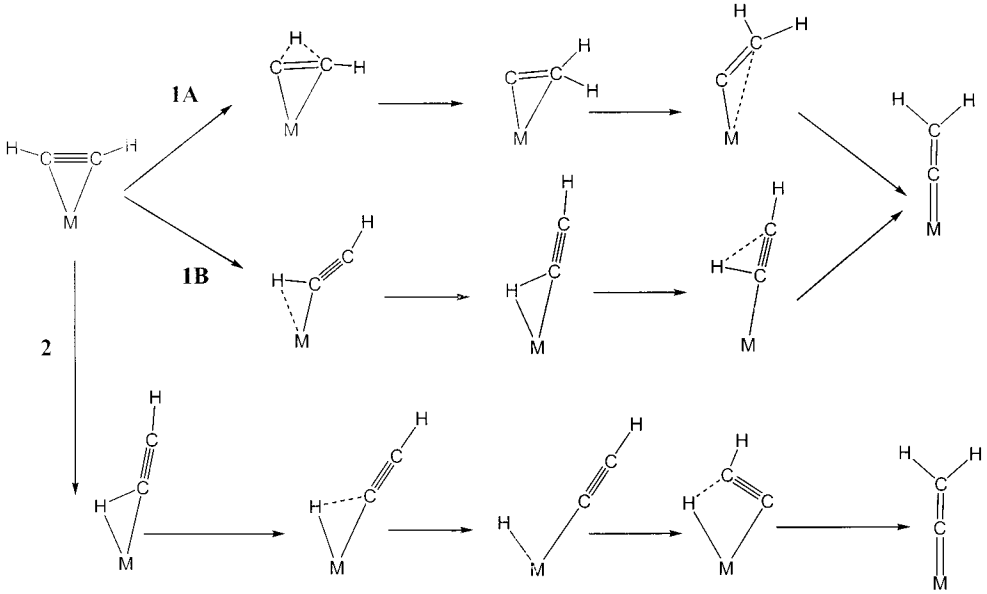

process to an intermediate species (path 1B in Scheme 1) showing an agostic interaction between the metal center and one C−H bond, which then undergoes the 1,2 hydrogen shift. A stationary state corresponding to the hypothetical alkynylhydrido intermediate $[Cl_2(PH_3)_2Ru(H)(-C{\equiv}CH)]^+$ was localized (path 2 in Scheme 1), but it was found very unstable so that the oxidative addition of acetylene is thermodynamically very unfavorable and path 2 was ruled out.

On the other hand, analogous calculations on the rhodium(I) d^8 $[Cl(PH_3)_2Rh(HC{\equiv}CH)]$ complex showed that in this case the rearrangement proceeds through a stable alkynylhydrido intermediate, which then leads to the vinylidene complex via an intermolecular process rather than an intramolecular 1,3 hydrogen shift, which is higher in energy.[8] Further calculations have been recently carried out on the acetylene−vinylidene rearrangement in indenyl−ruthenium(II) complexes,[9] but only path 1 was considered. Theoretical investigations were also performed on the same process, in d^2 metal complexes. García-Yebra et al. considered a niobium(III) $[(Cp)_2Nb(PH_3)(HC{\equiv}CMe)]^+$ system[10] and found that path 1B is favored over path 2, with energy barriers of 38.5 and 52.2 kcal mol^{-1}, respectively; on the other hand, Frenking et al. investigated a hypothetical tungsten(II) $[F_4W(HC{\equiv}CH)]$ complex, finding high energy barriers for both path 1A and path 2 (respectively 84.8 and 85.3 kcal mol^{-1}), suggesting that the acetylene−vinylidene rearrangement is quite unlikely for this system.[11]

Despite the experimental interest in the metal-assisted acetylene−vinylidene rearrangement, only four ab initio studies comparing pathways 1 and 2, notably on Ru(II), Rh(I), Nb(III), and W(II) species, have been performed and the prototype fragment for this rearrangement, $[Cp(CO)_2Mn]$, was investigated only at the extended Hückel level.[6]

In this paper we report gradient-corrected DFT calculations on the rearrangement of the $[Cp(CO)_2Mn(HC{\equiv}CH)]$ acetylene complex to the $[Cp(CO)_2Mn(=C=CH_2)]$ vinylidene tautomer. We have combined "static" DFT calculations on the stationary points of the potential surface with the first-principles molecular dynamics calculations based on the Car−Parrinello approach.[12] Static DFT calculations have been performed in order to compute the geometries and the relative stabilities of the stationary points of the potential energy surface for the acetylene to vinylidene rearrangement. Car−Parrinello simulations have been employed to study the hitherto inaccessible dynamic features of this process.

1.1. Computational Details. Static DFT Calculations. The static DFT and post-Hartree−Fock calculations reported in this paper have been performed using the Gaussian 98 program package.[13] We used a 6-311G** basis set[14−16] for all the atoms, for a total of 286 basis functions. Geometry optimizations were performed on all the stationary points of the potential energy surface for acetylene rearrangement considering the Vosko−Wilk−Nusair LDA parametrization[17] and including the Becke[18] and Perdew−Wang[19] gradient corrections (GC)

(8) Wakatsuki, Y.; Koga, N.; Werner, H.; Morokuma, K. *J. Am. Chem. Soc.* **1997**, *119*, 360.

(9) Cadierno, V.; Gamasa, M. P.; Gimeno, J.; Pérez-Carreño, E.; García-Granda, S. *Organometallics* **1999**, *18*, 2821. Cadierno, V.; Gamasa, M. P.; Gimeno, J.; González-Bernardo, C.; Pérez-Carreño, E.; García-Granda, S. *Organometallics* **2001**, *20*, 5177.

(10) García-Yebra C.; López-Mardomingo C.; Fajardo, M.; Antiñolo, A.; Otero, A.; Rodríguez A.; Vallat, A.; Lucas, D.; Mugnier, Y.; Carbó, J. J.; Lledós, A.; Bo, C. *Organometallics* **2000**, *19*, 1749.

(11) Stegmann, R.; Frenking, G. *Organometallics* **1998**, *17*, 2089.

(12) Car, R.; Parrinello, M. *Phys. Rev. Lett.* **1985**, *55*, 2471.

(13) Frisch, M. J.; Trucks, G. W.; Schlegel, H. B.; Scuseria, G. E.; Robb, M. A.; Cheeseman, J. R.; Zakrzewski, V. G.; Montgomery, J. A., Jr.; Stratmann, R. E.; Burant, J. C.; Dapprich, S.; Millam, J. M.; Daniels, A. D.; Kudin, K. N.; Strain, M. C.; Farkas, O.; Tomasi, J.; Barone, V.; Cossi, M.; Cammi, R.; Mennucci, B.; Pomelli, C.; Adamo, C.; Clifford, S.; Ochterski, J.; Petersson, G. A.; Ayala, P. Y.; Cui, Q.; Morokuma, K.; Malick, D. K.; Rabuck, A. D.; Raghavachari, K.; Foresman, J. B.; Cioslowski, J.; Ortiz, J. V.; Stefanov, B. B.; Liu, G.; Liashenko, A.; Piskorz, P.; Komaromi, I.; Gomperts, R.; Martin, R. L.; Fox, D. J.; Keith, T.; Al-Laham, M. A.; Peng, C. Y.; Nanayakkara, A.; Gonzalez, C.; Challacombe, M.; Gill, P. M. W.; Johnson, B. G.; Chen, W.; Wong, M. W.; Andres, J. L.; Head-Gordon, M.; Replogle, E. S.; Pople, J. A. *Gaussian 98*, revision A.7; Gaussian, Inc.: Pittsburgh, PA, 1998.

(14) Frisch, M. J.; Pople J. A.; Binkley, J. S. *J. Chem. Phys.* **1984**, *80*, 3265, and references therein.

(15) Hay, P. J. *J. Chem. Phys.* **1977**, *77*, 4377.

(16) Wachters, A. J. H. *J. Chem. Phys.* **1970**, *52*, 1033.

(17) Vosko, S. H.; Wilk, L.; Nusair, M. *Can. J. Phys.* **1980**, *58*, 1200.

(18) Becke, A. D. *Phys. Rev.* **1988**, *A38*, 3098.

to the exchange and correlation, respectively. The transition states were obtained by the synchronous transit-guided quasi-Newton method available in Gaussian 98.[20] All stationary points were optimized without any symmetry constraints; frequency calculations were performed on all the stationary points, and intrinsic reaction coordinate (IRC) analysis[21,22] has been performed on the computed transition state structures. Thermal corrections and entropy contributions were added to all energies so that the energetic data reported in the following are reaction free energies. Moreover, we checked the consistency of the CP and Gaussian98 DFT implementations and compare DFT results to post-Hartree−Fock MP2 [23] calculations.

Car−Parrinello Calculations. Molecular dynamics simulations were carried out with the Car−Parrinello (CP) method[12] for both path 1A and path 1B in Scheme 1. Gradient-corrected calculations have been performed using the parallel version, developed by one of us (F.D.A.), of the CP code implementing Vanderbilt pseudopotentials.[24,25] For the LDA exchange−correlation functional the Perdew−Zunger parametrization[26] has been used, while the gradient-corrected functional is taken from ref 27. Core states are projected out using pseudopotentials. For all the atoms "ultrasoft" pseudopotentials were generated according to the scheme proposed by Vanderbilt.[25] The wave functions were expanded in plane waves up to an energy cutoff of 25 Ry. Periodic boundary conditions were used by placing the model molecule in a cubic box of 10.6 Å, sufficiently large to avoid coupling between periodic images. The equations of motion were integrated using a time step of 6 au (0.145 fs) with an electronic fictitious mass $\mu = 500$ au. Constrained dynamics simulations were performed by means of the SHAKE algorithm,[28] employing the slow-growth method[29] in which the constrained parameter is slowly varied as a function of the simulation time, in such a way that the potential energy surface along the considered constraint is dynamically sampled; to maintain the system in thermal equilibrium, the temperature of the nuclei was controlled by a Nosé thermostat,[30] which creates a canonical (NVT) ensemble. All simulations were conducted at 300 K.

Calibration and Consistency of the Calculations. To check the consistency of the CP and Gaussian98 DFT implementations, we compared the geometries of the fully optimized vinylidene complex $(Cp)(CO)_2Mn(=C=CH_2)$, **2**, to those of the closest experimental compound for which X-ray data are available, i.e. the phenylvinylidene complex $(Cp)(CO)_2Mn(=C=CHPh)$.[5] In Table 1 optimized geometrical parameters computed with the CP and Gaussian98 DFT implementations have been reported and show a good agreement between the two DFT implementations and the experimental data. In particular, both the CP and Gaussian98 DFT approaches show very close distances within the Mn=C=C core, suggesting that the interactions between the metal and unsaturated ligands are accounted for with the same accuracy by both methods.

Table 1. Optimized Geometrical Parameters (Å and deg) Computed with the CP and Gaussian98 DFT Implementations, Compared with Experimental Data for the $(Cp)(CO)_2Mn(=C=CH_2)$ Vinylidene Complex 2[a]

parameter	CP	G98	exptl
r_{Mn-Cp} (av)	2.165	2.173	2.16(2)
r_{Mn-CO}	1.782	1.787	1.74(5)
r_{Mn-CC}	1.765	1.768	1.68(2)
r_{C-C}	1.316	1.315	1.34(3)
∠OC−Mn−CO	89.3	89.3	89(1)

[a] The experimental data refer to the $(Cp)(CO)_2Mn(=C=CHPh)$ complex.[5]

Table 2. ΔE and E_a Computed Using the CP and Gaussian98 DFT Implementations and at the MP2 Level on the Gaussian98 DFT Optimized Geometries, Both in Vacuo (upper panel) and in Methanol (lower panel, DFT only)[a]

parameter	CP	G98	MP2
ΔE	−10.7	−10.2	−13.4
E_a	46.1	47.4	48.2
ΔE	−9.5	−8.9	
E_a	44.2	44.6	

[a] ΔE refers to the nonthermal corrected energy difference between **1** and **2**, while E_a refers to the nonthermal corrected energy difference between **1** and $\mathbf{TS}_{1\to3}$. Energetics in solution are solvation free energies. Energy in kcal mol^{-1}.

To further support the consistency of CP and Gaussian98 DFT implementations and to compare DFT results to post-Hartree−Fock MP2 calculations, we reported the energetics obtained by performing single-point calculations on the Gaussian98 DFT optimized geometries with the three approaches, considering the energy difference between the starting reagent **1** and the final product **2** and between **1** and the transition state connecting **1** and **3**, $\mathbf{TS}_{1\to3}$, vide infra, indicated as ΔE and E_a, respectively. Moreover, to check whether environmental effects play a role in determining the overall energetics, we performed single-point calculations at the DFT level on the Gaussian98 DFT geometries optimized in vacuo of **1**, **2**, and $\mathbf{TS}_{1\to3}$ employing the C-PCM continuum solvation model due to Barone et al.,[31] which we recently contributed to implement in the CP framework.[32] We chose methanol, which has the highest dielectric constant ($\epsilon = 32.63$) among the experimentally employed solvents.

The results are collected in Table 2. As it can be noticed both CP and Gaussian98 DFT implementations result in quantitatively similar energetics, both in vacuo and in solution, suggesting that the potential energy

(19) Perdew, J. P.; Wang, Y. *Phys. Rev.* **1992**, *B45*, 13244.
(20) Simons, J.; Jorgensen, P.; Taylor H.; Ozment, J. *J. Phys. Chem.* **1983**, *87*, 2745.
(21) Gonzalez C.; Schlegel, H. B. *J. Chem. Phys.* **1989**, *90*, 2154.
(22) Gonzalez C.; Schlegel, H. B. *J. Phys. Chem.* **1990**, *94*, 5523.
(23) Møller C.; Plesset, M. S. *Phys. Rev.* **1934**, *46*, 618.
(24) The implementation that we use is described in: Pasquarello, A.; Laasonen, K.; Car, R.; Lee, C.; Vanderbilt, D. *Phys. Rev. Lett.* **1992**, *69*, 1982; Pasquarello, A.; Laasonen, K.; Car, R.; Lee, C.; Vanderbilt, D. *Phys. Rev. B* **1993**, *47*, 10142.
(25) Vanderbilt, D. *Phys. Rev. B* **1990**, *41*, 7892.
(26) Perdew, J. P.; Zunger, A. *Phys. Rev. B* **1981**, *23*, 5048.
(27) Perdew, J. P.; Chevary, J. A.; Vosko, S. H.; Jackson, K. A.; Pederson, M. R.; Singh, D. J.; Fiolhais, C. *Phys. Rev. B* **1992**, *46*, 6671.
(28) Ryckaert, J. P.; Ciccotti, G.; Berendsen, H. J. *J. Comput. Phys.* **1977**, *23*, 327.
(29) Straatsma, T. P.; Berendsen, H. J. C.; Postma, J. P. M. *J. Chem. Phys.* **1986**, *85*, 6720.
(30) Nosé, S. *Mol. Phys.* **1984**, *52*, 255. Hoover, W. G. *Phys. Rev. A* **1985**, *31*, 1695.
(31) Barone V.; Cossi, M.; Tomasi, J *J. Comput. Chem.* **1998**, *19*, 404.
(32) De Angelis, F.; Sgamellotti, A.; Cossi, M.; Rega, N.; Barone, V. *Chem. Phys. Lett.* **2000**, *328*, 302.

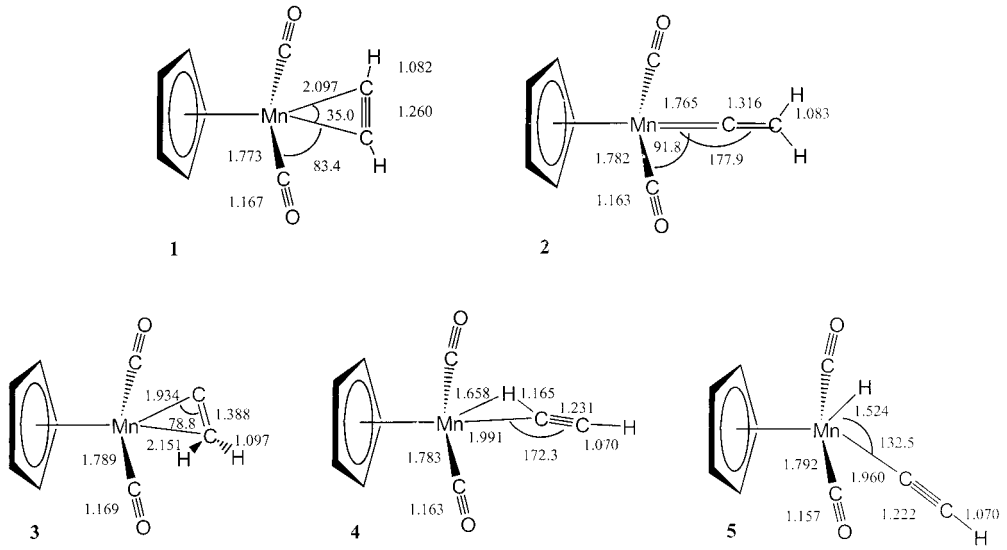

Figure 1. Structures and main optimized geometrical parameters (Å, deg) for the acetylene **1**, vinylidene **2**, η^2-bound vinylidene **3**, η^2-C−H agostic acetylene **4**, and alkynylhydrido **5**, complexes.

surfaces are indeed quite similar within the two DFT approaches. Moreover, DFT barriers for hydrogen transfer are in good agreement with the MP2 result, with only a small underestimate (less than 3 kcal mol^{-1}). This is a clear indication that in the present case we can trust in the DFT barrier heights. Finally, since solvation is shown to have a minor impact on the overall energetics, we did not include it in the following results.

2. Results and Discussion

Preliminary calculations have been performed on the rearrangement of free acetylene to vinylidene, and an energy difference of 44.5 kcal mol^{-1} has been computed, in excellent agreement with the experimental value of 44−47 kcal mol^{-1}.[2] We then started our analysis by searching equilibrium structures on the potential energy surface of the C_2H_2 unit bound to the $Cp(CO)_2Mn$ fragment. We have found altogether five minima, i.e., the acetylene complex **1**, the vinylidene complex **2**, an η^2-bound vinylidene complex **3**, an η^2-C−H coordinated acetylene complex **4**, and an alkynylhydrido complex **5**. Structures and main geometrical parameters for complexes **1**−**5** can be found in Figure 1. The vinylidene complex **2** is found as the global energy minimum structure and is 9.0 kcal mol^{-1} lower than the acetylene complex **1**. The computed metal−carbon (Mn−C_α) and carbon−carbon (C_α−C_β) distances are 1.765 and 1.316 Å, respectively, for **2** and 2.097 and 1.260 Å for **1**, reflecting the changes of the bond orders in these complexes. A careful inspection of path 1A (see below) has revealed the presence of an unusual η^2-bound vinylidene complex, **3**, which is 38.4 kcal mol^{-1} higher than the most stable η^1-bound isomer **2**. A stable minimum corresponding to an η^2-C−H coordination of the acetylene moiety to the metal, **4**, was found 13.6 kcal mol^{-1} higher in energy than **1**; such a species is characterized by an agostic interaction between the metal center and one C−H bond, as suggested by the values of the Mn−H and Mn−C_α distances of 1.658 and 1.991 Å, with an almost linear (172.3°) ∠Mn−C_α−C_β angle. This η^2-C−H coordinated species is the natural precursor of the oxidative addition of the acetylene C−H bond to the metal center, leading to an alkynylhydrido complex (path 2). Indeed, starting from the geometry of complex **4**, we performed a linear transit scan of the potential energy surface assuming the ∠HMnC_α angle as a reaction coordinate (RC), localizing the alkynylhydrido complex **5** 6.1 kcal mol^{-1} higher in energy than **4**, for a value of the ∠HMnC_α angle close to 132°. The Mn−H and Mn−C_α distances are computed 1.524 and 1.960 Å, respectively, with a linear (179.2°) ∠Mn−C_α−C_β angle.

2.1. Pathway 1A. To gain some insight into the reaction mechanisms leading to the formation of the vinylidene complex **2** and to provide a guess for the transition state structures connecting the various minima on the reactive potential energy surface, we performed constrained molecular dynamics simulations starting from complex **1**. We choose to constrain the C_β−H distance, expecting this parameter to connect the reagent and the product basins, by varying it from a value of 2.2 Å corresponding to **1** to 1.1 Å, corresponding to **2**, as a function of the simulation time. The total time span of the simulation was 10 ps.

A point that needs to be stressed here is that we only mean to exploit the power of molecular dynamics to sample the potential energy surface without performing any thermodynamical integration along the approximate RC; indeed, such a procedure can be reasonably accurate only if the approximate RC has a high projection onto the reaction mode and would be better performed considering a constrained motion of the system along a predetermined multidimensional intrinsic reaction pathway, as recently suggested by Michalak et al.[33]

The evolution of the hydrogen shift can be followed by studying the time evolution of C_α−H and of the C_β−Mn distances. Indeed, the C_α−H distance is ca. 1.1 Å in the reagent **1**, where the H atom is directly bound to the α carbon, while it grows up to ca. 2.2 Å in the product **2**, where they are no longer bound. On the other hand, the C_β−Mn distance is ca. 2.1 Å in **1**, growing to ca. 3.1 Å in **2**, reflecting the detaching of the β carbon

(33) Michalak, A.; Ziegler, T. *J. Phys. Chem. A* **2001**, *17*, 4333.

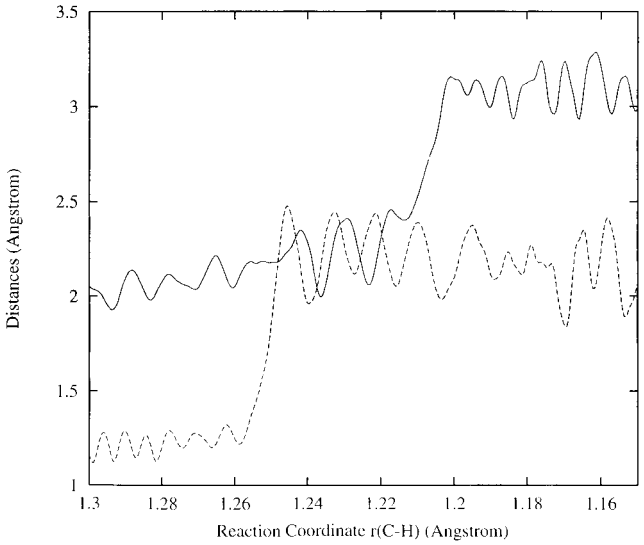

Figure 2. Time evolution of the $C_\alpha-H$, dashed line, and $C_\beta-Mn$, solid line, distances (Å) for the dynamics simulation starting from the acetylene complex **1** in the RC range 1.30−1.15 Å (8−9 ps).

from the metal. To analyze the reaction mechanism in better detail, Figure 2 displays the variation of the considered parameters as a function of the RC only in the range 1.30−1.15 Å, corresponding to the time span going from 8 to 9 ps. As it can be noticed, a 1,2-shift takes place for an RC value close to 1.26 Å, as suggested by the fast increase in the $C_\alpha-H$ distance observed between 1.26 and 1.24 Å; thereafter, this parameter continues to oscillate around 2.2 Å, a value characteristic of the vinylidene complex **2**. It is interesting to note how the $C_\beta-Mn$ distance exhibits a similar behavior, even if its increase to ca. 3.1 Å, characteristic of complex **2**, is delayed by ca. 0.04 Å along the RC axis, corresponding to ca. 0.4 ps in time, suggesting that the 1,2-shift takes place prior to decoordination of the β carbon from the metal, therefore indicating the presence of a transient η^2-bound vinylidene species, **3**. The short time stability of complex **3**, ca. 0.4 ps, suggests that a small energy barrier connects **3** to the more stable η^1-bound vinylidene **2**. Moreover, we did not observe the formation of the η^2-C−H acetylene species **4**, suggesting that a direct 1,2-shift is indeed a viable pathway to the formation of **2**.

Motivated by these results, we optimized the geometry of the η^2-bound vinylidene **3**, finding it to be a real minimum on the potential energy surface, 38.4 kcal mol^{-1} higher in energy than the η^1-bound isomer **2** and 29.4 kcal mol^{-1} above **1**. Structure and main geometrical parameters for complex **3** can be found in Figure 1. To the best of our knowledge an η^2-bound vinylidene species has never been detected, all structurally characterized vinylidene complexes assuming the usual η^1-coordination mode. It is worth analyzing the bonding interactions in this unusual η^2-bound vinylidene complex and to compare them with those for the more stable η^1-isomer, which have been analyzed for a long time.[34] The frontier orbitals of the $Mn(Cp)(CO)_2$ fragment involved in the interactions with the vinylidene moiety

Scheme 2

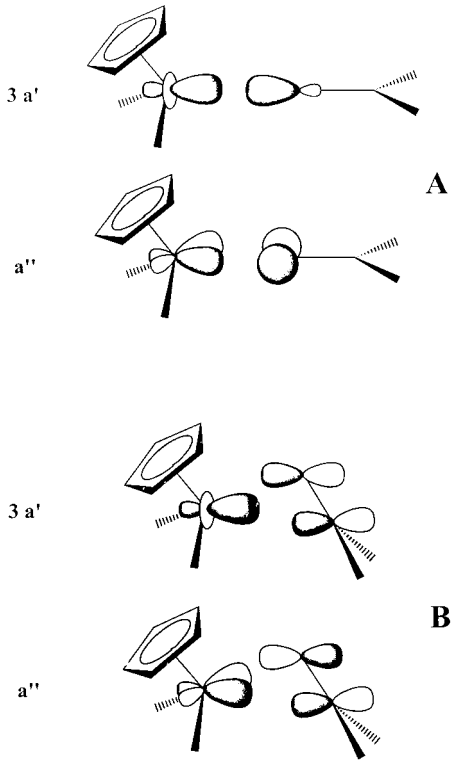

are the LUMO 3a′, mainly a d_{z^2}, and the HOMO a″, mainly a d_π orbital lying in a plane perpendicular to the symmetry plane bisecting the fragment (see Scheme 2). In the η^1-species the vinylidene lone pair on the C_α donates into the empty 3a′ orbitals, while the a″ orbital back-donates its electrons in the empty 2p(π) AO on the C_α of vinylidene, A in Scheme 2. On the other hand, in the η^2-species the donation occurs between the filled vinylidene π orbital to the empty 3a′ orbitals, while the a″ orbital back-donates its electrons in the empty π^* orbital of vinylidene, B in Scheme 2. As a consequence of these different orbital interactions, in the η^2-species the vinylidene moiety lies perpendicularly to the fragment symmetry plane (as in the acetylene complex) and the C−C bond distance is more elongated than in the η^1-species (1.388 vs 1.316 Å) (see Figure 1).

By extracting selected snapshots from the dynamics simulation we were able to locate the transition state, $\mathbf{TS}_{1\to3}$, corresponding to the conversion between **1** and **3**, finding a structure 45.3 kcal mol^{-1} higher than **1**; the transition state, $\mathbf{TS}_{3\to2}$, corresponding to the conversion between **3** and **2** was found only 2.5 kcal mol^{-1} above **3**, in agreement with the short time stability of such a species observed during the dynamics simulations. A schematic representation of the potential energy surface for the overall direct 1,2-shift has been reported in Figure 3, from which it appears that formation of **3** is the rate-determining step. Structures of $\mathbf{TS}_{1\to3}$ and $\mathbf{TS}_{3\to2}$, together with main geometrical parameters, have been reported in Figure 4. It is interesting to note that the geometry of the metal−C_2H_2 core of $\mathbf{TS}_{1\to3}$ partially resembles that found for the d^2 [F_4W(HC≡CH)] system,[11] with an out-of-plane configuration of the migrating hydrogen. Such an out-of-plane migration of the hydrogen is necessary because of the partial occupation of the in-plane p(π) AO of the C_β atom on the

(34) Schilling, B. E. R.; Hoffmann, R.; Lichtenberger, D. L. *J. Am. Chem. Soc.* **1979**, *101*, 585. Kostic, N. M.; Fenske, R. F. *Organometallics* **1982**, *2*, 974.

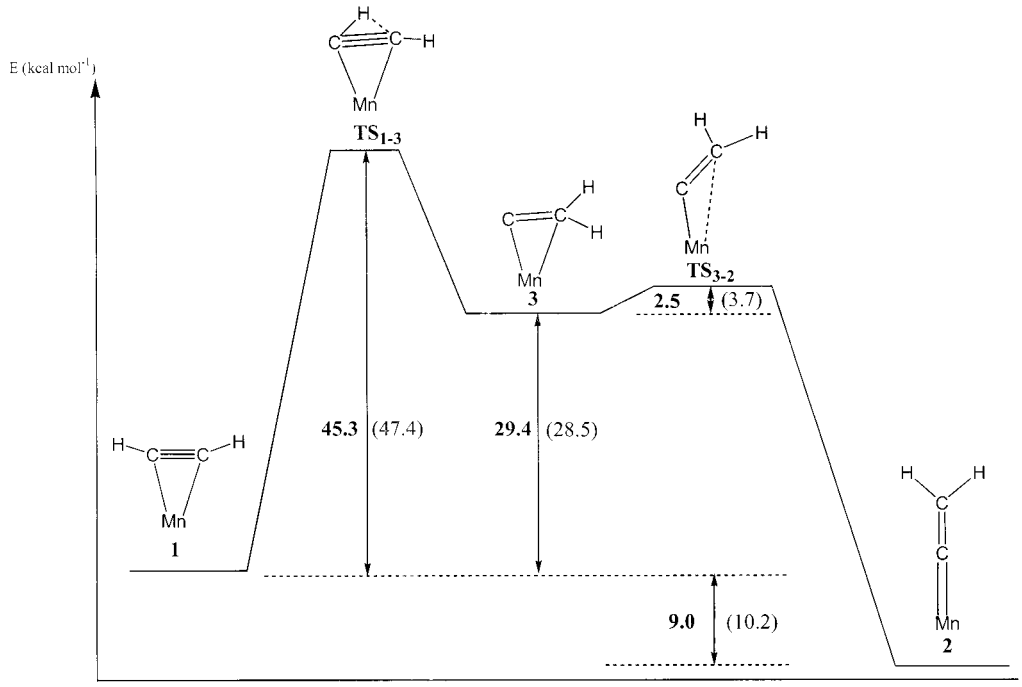

Figure 3. Schematic representation of the potential free energy surface for the direct 1,2 hydrogen shift (pathway 1A). The data in parentheses refer to nonthermal corrected energies. Energy in kcal mol^{-1}.

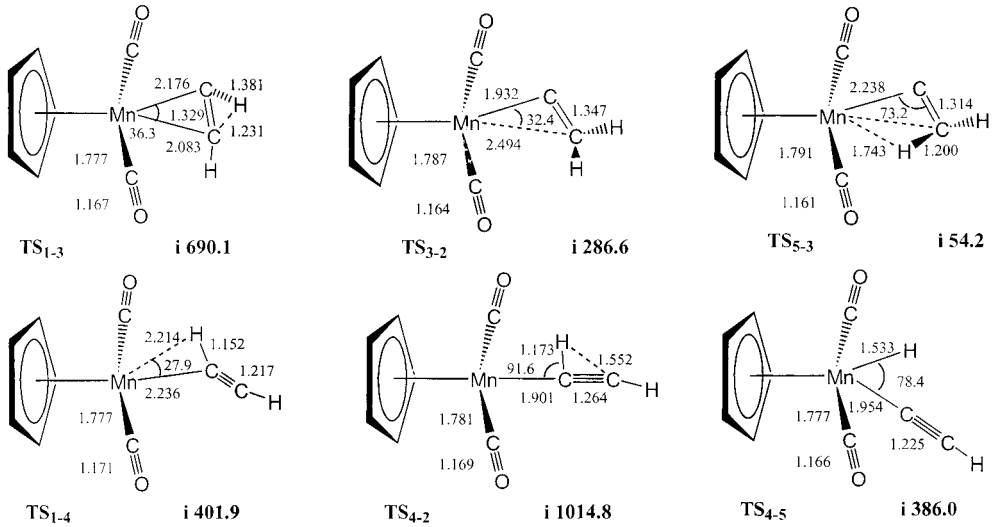

Figure 4. Structures and main optimized geometrical parameters (Å, deg) for the transition states connecting the equilibrium structures **1**−**5**.

incipient moiety due to back-donation from the metal d_π orbital,[11] and, indeed, no transition state with an in-plane configuration of the migrating hydrogen could be found. No out-of-plane transition states were found by Morokuma and co-workers for the d^6 $[Cl_2Ru(PH_3)_2(HC{\equiv}CH)]^+$ and the d^8 $[Cl(PH_3)_2Rh(HC{\equiv}CH)]$ systems,[7,8] probably because their calculations were performed within C_s symmetry constraints. A comparison between the out-of-plane transition states for the direct 1,2 hydrogen shift in the d^2 $[F_4W(HC{\equiv}CH)]$[11] and our d^6 manganese system shows that in the latter case the transition state structure is more symmetric than that of ref 11, with C$_\alpha$−H and C$_\beta$−H distances of 1.381 and 1.231 Å as opposed to 1.730 and 1.140 Å, respectively.

2.2. Pathway 1B. To rationalize the role played by complex **4** in the formation of **2**, we performed constrained dynamics simulations starting from **4**, employing the same methodology already applied to **1**, vide supra. We therefore constrained the C$_\beta$−H distance to vary from a value of 2.2 Å, corresponding to **4**, to 1.1 Å, corresponding to **2**, as a function of the simulation time. The total time span of the simulation was 10 ps. The evolution of the hydrogen shift can be followed by studying the time evolution of C$_\alpha$−H and of the Mn−H distances. Indeed, the C$_\alpha$−H distance is ca. 1.1 Å in complex **4**, where the H atom is directly bound to the α carbon, while it grows to ca. 2.1 Å in the product **2**, where they are no longer bound. On the other hand, the Mn−H distance is ca. 1.7 Å in **4**, growing to ca. 3.8 Å in **2** as a consequence of the hydrogen shift to the β carbon. Figure 5 displays the variation of the considered parameters as a function of the RC for the entire range of the RC. As it can be noticed, the hydrogen shift takes place for an RC value close to 1.42 Å, as suggested by

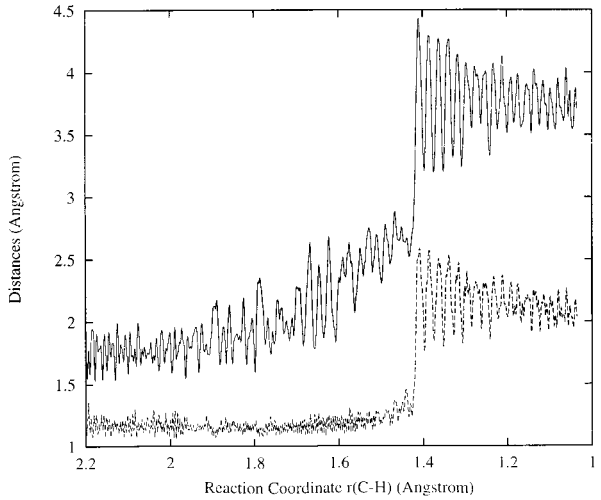

Figure 5. Time evolution of the Mn−H, solid line, and C_α−H, dashed line, distances (Å) for the dynamics simulation starting from the η^2-C−H agostic acetylene complex **4** in the RC range 2.20−1.10 Å (0−10 ps).

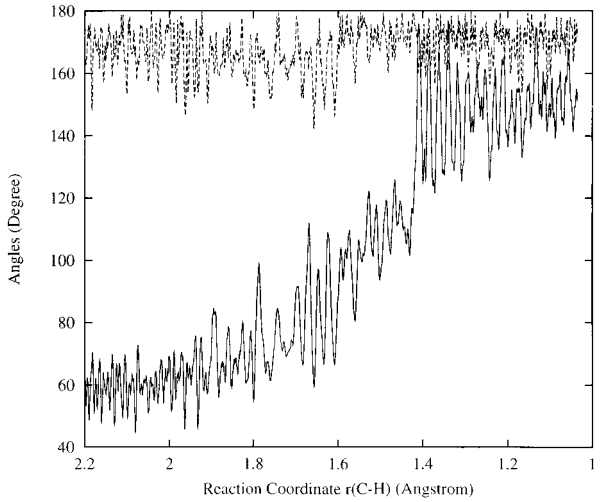

Figure 6. Time evolution of the H−C_α−Mn, solid line, and Mn−C_α−C_β, dashed line, angles (deg) for the dynamics simulation starting from the η^2-C−H agostic acetylene complex **4** in the RC range 2.20−1.10 Å (0−10 ps).

the fast increase in the C_α−H distance observed between 1.42 and 1.40 Å. From Figure 5 we can notice that the hydrogen detachment from the metal takes place prior to hydrogen migration, suggesting a transition state in which the decoordinated H atom is still exploiting the bonding interaction with the α carbon. Figure 6 displays the evolution of the ∠HC_αMn and of the ∠$MnC_\alpha C_\beta$ angles as a function of the RC. The evolution of the ∠HC_αMn angle follows a similar trajectory to the Mn−H distance, reflecting the H decoordination from the metal prior to migration, which we have already identified to take place for a value of the RC of ca. 1.40 Å. Moreover, we can observe that the 1,2-shift does not affect the ∠$MnC_\alpha C_\beta$ angle, which remains approximatively linear along the whole time evolution and shows reduced oscillations after 1.40 Å, suggesting that the transition state structure is stabilized by the partial formation of the incoming double metal−carbon bond, which makes the ∠$MnC_\alpha C_\beta$ angle stiffer.

By extracting selected snapshots from the dynamics simulation we optimized the transition state $\mathbf{TS}_{4\rightarrow2}$, corresponding to the conversion between **4** and **2**, finding a structure 13.7 kcal mol^{-1} higher than **4** and therefore 27.3 kcal mol^{-1} above **1**. Moreover, we could also locate the transition state structure $\mathbf{TS}_{1\rightarrow4}$, corresponding to the slippage process from **1** to **4**, finding it 25.3 kcal mol^{-1} higher than **1**. A schematic representation of the potential energy surface for the overall hydrogen shift in path 1B has been reported in Figure 7; as it can be noticed the highest barrier to the formation of **2** is computed to be only 27.3 kcal mol^{-1}, i.e., 18 kcal mol^{-1} lower than the value computed for the direct 1,2-shift of path 1A. Structures of $\mathbf{TS}_{1\rightarrow4}$ and $\mathbf{TS}_{4\rightarrow2}$, together with main geometrical parameters, have been reported in Figure 4. As it can be noticed, the $\mathbf{TS}_{4\rightarrow2}$ structure shows a reduced value of the Mn−C_α bond with respect to **4** (1.901 vs 1.991 Å), a slight increase in the $C_\alpha C_\beta$ distance (1.264 vs 1.231 Å), and an increased value of the ∠$HMnC_\alpha$ angle (97.6° vs 56.2°), confirming the picture extracted from the dynamics simulations; moreover, the C_α−H and C_β−H distances are computed to be 1.173 and 1.552 Å, reflecting the tendency of the migrating H atom to exploit the bonding interaction with the α carbon.

3. Pathway 2. Since a pseudo-octahedral alkynylhydrido d^4 species would be expected to have a triplet ground state, we checked whether higher spin configurations play a role in determining the energetics of path **2** and optimized the geometry of the alkynylhydrido complex **5**, imposing singlet, triplet, and quintet spin-multiplicities, finding a singlet ground state, with the triplet 36.6 kcal mol^{-1} higher in energy, and the quintet still 22.3 kcal mol^{-1} higher. Therefore, starting from the maximum energy structure encountered during the linear transit procedure on the singlet surface, vide supra, we localized the transition state, $\mathbf{TS}_{4\rightarrow5}$, for the oxidative addition leading from the agostic intermediate **4** to the alkynylhydrido complex **5**, finding a structure 21.4 kcal mol^{-1} above **4**, therefore 35.0 kcal mol^{-1} above the acetylene complex **1**. For the sake of completeness, we also reoptimized $\mathbf{TS}_{4\rightarrow5}$, imposing a triplet spin-multiplicity, finding it 20.6 kcal mol^{-1} above the singlet optimized transition state structure. We can therefore rule out the participation of higher spin energy surfaces in the investigated process. $\mathbf{TS}_{4\rightarrow5}$ shows a formed Mn−H and a broken C_α−H bond (1.533 and 2.228 Å, respectively), with a ∠$HMnC_\alpha$ angle of 78.4° (see Figure 4). The computed energy barrier is 7.7 kcal mol^{-1} higher than that for the 1,2-shift from the agostic intermediate **4**, so that the intermediacy of **5** in the formation of **2** seems unlikely.

We finally localized the transition state corresponding to the 1−3 hydrogen shift leading from **5** to **3**, finding a structure, $\mathbf{TS}_{5\rightarrow3}$, 25.8 kcal mol^{-1} above **5**, therefore 45.5 kcal mol^{-1} above **1**, suggesting that an eventual alkynylhydrido to vinylidene rearrangement would probably follow an intermolecular rather than an intramolecular pathway, as found by Morokuma for the [Cl-$(PH_3)_2$Rh(HC≡CH)] system.[8] The structure of $\mathbf{TS}_{5\rightarrow3}$ (see Figure 4) shows an η^2-coordination mode of the forming vinylidene (∠$MnC_\alpha C_\beta$ = 73.2°), with an elongated Mn−H distance (1.743 Å) and an almost formed C−H bond (1.200 Å), suggesting that $\mathbf{TS}_{5\rightarrow3}$ correlates with the η^2-vinylidene species **3**, rather than with the more stable η^1-vinylidene **2**, to which **3** is connected by

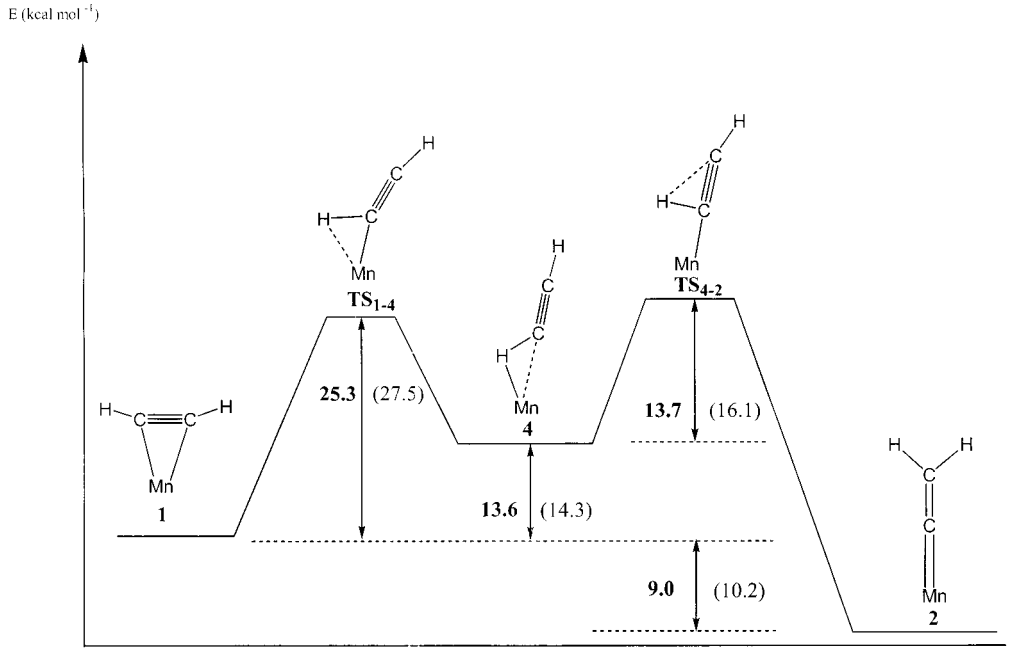

Figure 7. Schematic representation of the potential free energy surface for the 1,2 hydrogen shift passing through the η^2-C−H agostic species (pathway 1B). The data in parentheses refer to nonthermal corrected energies. Energy in kcal mol^{-1}.

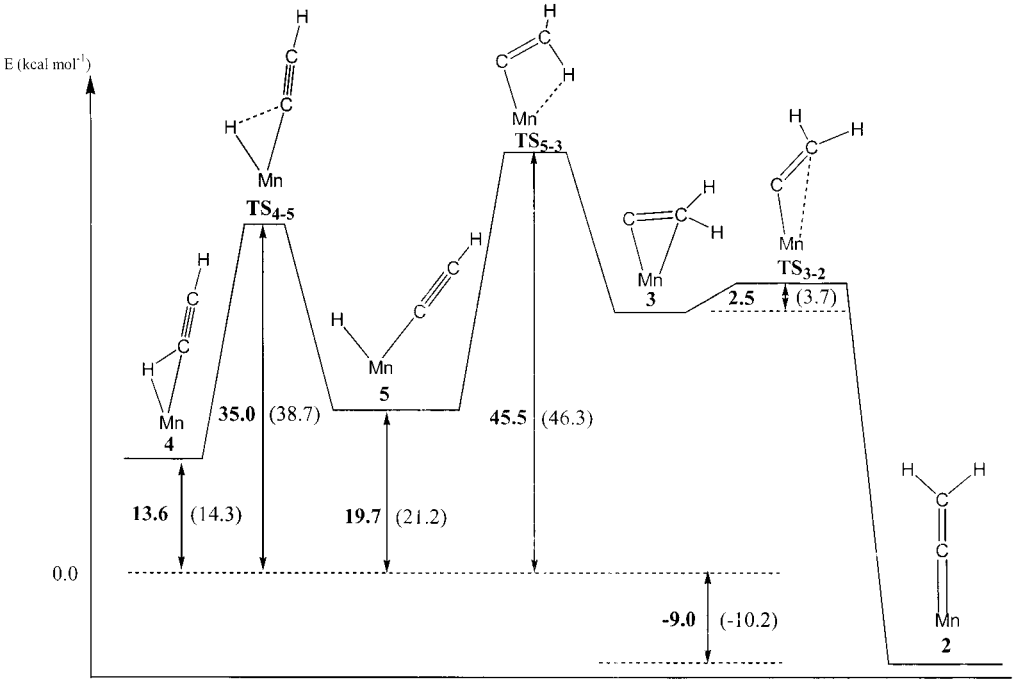

Figure 8. Schematic representation of the potential free energy surface for the 1,3 hydrogen shift passing through the alkynylhydrido species (pathway 2). The data in parentheses refer to nonthermal corrected energies. Energy in kcal mol^{-1}.

TS$_{3\rightarrow2}$. A schematic representation of the potential energy surface for the intermolecular 1,3-hydrogen shift in path **2** has been reported in Figure 8.

It is worth comparing the potential energy surface for the two-step pathway **1B** with that calculated by Morokuma and co-workers for the same reaction sequence of the analogous d^6 $[Cl_2Ru(PH_3)_2(HC{\equiv}CH)]^+$ system considering the rotational isomers correlating with the experimental monosubstituted acetylenes. The potential energy surfaces are, indeed, quite similar, with the vinylidene complex slightly lower than the acetylene one (9.0 kcal mol^{-1} for Mn, 8.7 kcal mol^{-1} for Ru), the η^2-C−H agostic intermediate moderately higher than the acetylene complex (14.3 kcal mol^{-1} for Mn, 13.6 kcal mol^{-1} for Ru), and the transition state for the conversion from the η^2-C−H agostic species to the vinylidene complex higher than the transition state for the slippage from the acetylene to the η^2-C−H agostic complex (25.3 and 27.3 kcal mol^{-1} for Mn, 17.7 and 37.3 kcal mol^{-1} for Ru). It is also worth noting that in the $[Cl_2Ru(PH_3)_2(HC{\equiv}CH)]^+$ complex the alkynylhydrido product, although still a minimum of the potential energy surface, is so high in energy (almost 100 kcal mol^{-1} above the acetylene complex) that it rules out pathway 2 in such

a ruthenium system. In the considered Mn(I) system a relatively stable alkynylhydrido species is found; however, the higher energy barrier computed for the oxidative addition in the present case with respect to the 1,2-shift taking place from **4** (35.0 vs 27.3 kcal mol^{-1}) makes unlikely the intermediacy of an alkynylhydrido species.

4. Conclusions

The isomerization of the $[Cp(CO)_2Mn(HC{\equiv}CH)]$ acetylene complex to the $[Cp(CO)_2Mn(=C{=}CH_2)]$ vinylidene tautomer has been investigated combining "static" DFT calculations on the stationary points of the potential surface with the first-principles molecular dynamics calculations based on the Car−Parrinello approach.

Five minima were found on the potential energy surface of the C_2H_2 unit bound to the $Cp(CO)_2Mn$ fragment, i.e., the acetylene complex **1**, the vinylidene complex **2**, an unprecedented η^2-bound vinylidene complex **3**, an η^2-C−H coordinated acetylene complex **4**, and an alkynylhydrido complex **5**. The vinylidene complex **2** has been found as the global energy minimum structure and is 9.0 kcal mol^{-1} lower than the acetylene complex **1**.

The potential energy surfaces for all three different pathways proposed for this metal-assisted isomerization, i.e., the direct 1,2 hydrogen shift from C_α to C_β (path 1A), the 1,2 hydrogen shift passing through an η^2-C−H agostic intermediate (path 1B), and the 1,3 rearrangement step passing through an alkynylhydrido intermediate (path 2), have been theoretically evaluated. The results indicate that the highest energy barrier for the 1,2 hydrogen shift passing through an η^2-C−H agostic intermediate (path 1B), 27.3 kcal mol^{-1}, is lower than the value computed both for the direct 1,2-shift of path 1A, 45.3 kcal mol^{-1}, and for the oxidative addition taking place prior to the intramolecular 1,3-shift of path 2, 35.0 kcal mol^{-1} and 45.5 kcal mol^{-1}, respectively. For the favored path 1B dynamics simulations have shown that the hydrogen detachment from the metal takes place prior to hydrogen 1,2-shift, suggesting that the decoordinated H atom exploits the bonding interaction with the α carbon throughout the migration process.

In conclusion, the higher energy barrier computed for the oxidative addition in the present case with respect to the 1,2-shift taking place from **4** (35.0 vs 27.3 kcal mol^{-1}) rules out the intermediacy of an alkynylhydrido species in the investigated process.

Acknowledgment. Thanks are due to the CNR (Progetto Finalizzato "Materiali Speciali per Tecnologie Avanzate II") for financial support.

OM010943K